

Enhancing search efficiency through diffusive echo

Charles Antoine¹ and Julian Talbot¹

Laboratoire de Physique Théorique de la Matière Condensée, UPMC, CNRS UMR 7600, Sorbonne Universités, 4, place Jussieu, 75252 Paris Cedex 05, France

(*Electronic mail: talbot@lptmc.jussieu.fr)

(*Electronic mail: charles.antoine@sorbonne-universite.fr)

(Dated: 23 May 2022)

Despite having been studied for decades, first passage processes remain an active area of research. In this contribution we examine a particle diffusing in an annulus with an inner absorbing boundary and an outer reflective boundary. We obtain analytic expressions for the joint distribution of the hitting time and the hitting angle in two and three dimensions. For certain configurations we observe a “diffusive echo”, i.e. two well-defined maxima in the first passage time distribution to a targeted position on the absorbing boundary. This effect, which results from the interplay between the starting location and the environmental constraints, may help to increase the efficiency of the random search by generating a sustained flux to the targeted position over a short period. Finally, we examine the corresponding one-dimensional system for which there is no well-defined echo.

I. INTRODUCTION

What is the probability that a diffusing agent arrives ‘alive’ at a specific target inside a highly constrained and hazardous environment? This question is pertinent in a wide range of fields from cellular biology and chemical reactions, to materials science, animal foraging and spreading of viruses^{1–10}. Examples include DNA and mRNA polymers diffusing passively inside the cell cytoplasm with the task of safely finding a nuclear pore to enter the cell nucleus^{11–15}. Or, more generally, for any brownian search process in a confined environment where traps or lethal zones may terminate the particle trajectory^{16–21}.

The outcome depends on many factors including the system geometry, the boundary conditions, the shape and mobility of the searcher and the target, the number and starting position of the searching agents, and the degree of hindrance due to crowding and possible traps. If the targeted site is behind an absorbing obstacle, one may wonder where to start the diffusive search process in order to optimize its efficiency. Too close to the obstacle, and the brownian trajectory will likely be killed before reaching its destination. Too far, and the diffusive exploration lengthens in a prohibitive way.

The presence of a boundary may radically affect the search, whether or not it is diffusive. In the context of sound propagation for example, a confining wall may reflect a distant voice, creating one or multiple echos.

For diffusive search processes, one no longer has a sound-like propagation but the question of a ‘diffusive echo’ effect is open. If it exists - and we show it does - one may wonder how it depends on the various parameters of the system and how it may enhance search efficiency. Of particular interest is the question of its persistence for a strong confinement in one, two and three dimensions.

The term ‘diffusive echo’ was first introduced in 1994 for steady two-dimensional flows^{22,23}. The effect is, however, tenuous, consisting of a subtle alteration of the transit time distribution at long times. More specifically, a shoulder is present between the usual power law decay at short times and the confinement-induced exponential decay at long times.

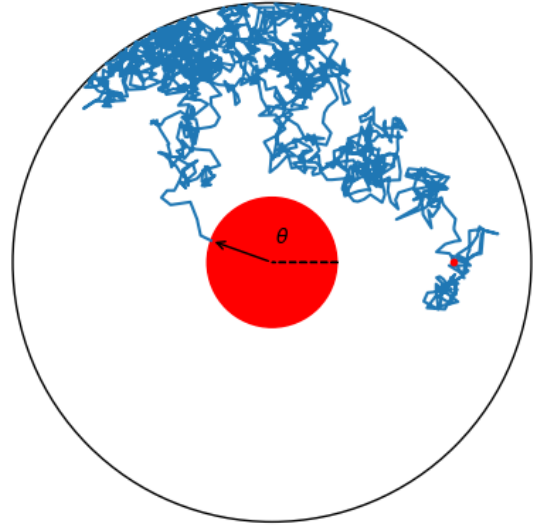


FIG. 1. The 2D system consists of a Brownian particle diffusing in an annulus formed from an inner absorbing disk of radius $a = 1$ and an outer reflecting wall of radius b (here equal to 4 for illustration). The diffusive particle trajectory starts at a distance r_0 from the center (small red point) and terminates when it touches the inner disk. The targeted position is labeled by the angle θ , while the starting position corresponds to $\theta = 0$.

This, however, cannot be considered as a true echo phenomenon, like the acoustic one, where two or more well defined maxima appear successively.

Geometric confinement is known to play a crucial role in first passage processes^{24–29}, be the external boundary totally or partially reflecting^{30,31}, with narrow^{32–34} or large escape zones and/or absorbing areas, part of which may play the role of target. Among notable recent applications of such confined processes, we can cite intracellular targeting for therapeutic intervention on oncogenic and degenerative diseases^{35–43}.

Diffusion phenomena, including heat transfer, are described theoretically by solving differential equations with the appro-

priate boundary conditions. The methodology, as well as solutions for many simple models, were established a long time ago^{44–46}, and underlie ongoing research^{25,26,28–31,47–52}.

In this article we consider the model shown in Fig. 1 where a spherical absorbing surface of radius a is contained within a spherically symmetric reflecting wall of radius b . The trajectory of a diffusing particle ends the instant it touches the inner, absorbing surface (perfect reactivity). In this work we are concerned with the joint probability that the diffusing particle hits a specific position on the central absorbing surface at time t . We first consider the two-dimensional case and then compare with the corresponding one and three dimensional systems.

II. TIME DEPENDENT HITTING DISTRIBUTION IN TWO DIMENSIONS

We seek the time-dependent hitting distribution at a specific position on the inner absorbing surface. This quantity, also known as first passage time distribution, may be obtained from the diffusive flux, which is proportional to the gradient of the particle concentration.

For the two dimensional problem, the time-dependent density evolves according to

$$D \left(\frac{1}{r} \frac{\partial}{\partial r} \left(r \frac{\partial c}{\partial r} \right) + \frac{1}{r^2} \frac{\partial^2 c}{\partial \theta^2} \right) = \frac{\partial c}{\partial t} \quad (1)$$

with absorbing and reflecting boundaries at $r = a$ and $r = b$, respectively:

$$\begin{aligned} c(a, \theta, t) &= 0, \\ \left. \frac{\partial c}{\partial r} \right|_{r=b} &= 0, \end{aligned} \quad (2)$$

and the initial condition

$$c(r, \theta, 0) = \frac{1}{r} \delta(r - r_0) \delta(\theta - \theta_0) \quad (3)$$

The diffusion coefficient D is assumed to be homogeneous and constant. The flux on a $d\theta$ wedge of the target is simply equal to $ad\theta D \left. \frac{\partial c}{\partial r} \right|_{r=a}$, leading to the time-dependent hitting distribution

$$j(\theta, t) = a D \left. \frac{\partial c}{\partial r} \right|_{r=a} \quad (4)$$

where the coordinate θ labels the targeted position on the inner circle, while the starting position corresponds to $\theta_0 = 0$.

To solve Eq. (1) we assume a solution of the form $c(r, \theta, t) = R(r)\Theta(\theta)T(t)$. This leads to an ordinary differential equation for the radial function

$$R'' + \frac{1}{r}R' + \left(k^2 - \frac{m^2}{r^2} \right) R = 0 \quad (5)$$

which can be expressed in terms of Bessel functions.

As detailed in Appendix B, the full solution of Eq. (1), which is periodic in θ and which satisfies the boundary conditions Eq. (2), is

$$c(r, \theta, t) = \frac{\pi}{2} \sum_{m=-\infty}^{\infty} \sum_{n=1}^{\infty} \cos(m\theta) \frac{F_{mn}(r)F_{mn}(r_0)}{C_{mn}} k_{mn}^2 e^{-k_{mn}^2 D t} \quad (6)$$

with the F_{mn} function defined as

$$F_{mn}(r) = Y_m(k_{mn}r)J_m(k_{mn}a) - J_m(k_{mn}r)Y_m(k_{mn}a) \quad (7)$$

where $J_m(x)$ and $Y_m(x)$ are the Bessel functions of the first and second kind, respectively, and k_{mn} is the n th root of the auxiliary equation

$$\begin{aligned} &J_m(ka)(Y_{m-1}(kb) - Y_{m+1}(kb)) \\ &= Y_m(ka)(J_{m-1}(kb) - J_{m+1}(kb)) \end{aligned} \quad (8)$$

for $m \geq 1$ and

$$J_0(ka)Y_1(kb) - Y_0(ka)J_1(kb) = 0 \quad (9)$$

for $m = 0$. These roots do not depend on the initial position r_0 and depend solely on m and the boundary positions a and b . The expression for the coefficients C_{mn} is given in the Appendix B. Note that Eq. (6) is symmetric in r and r_0 , and depends on these two positions only through the function F_{mn} .

The instantaneous flux at time t on the target at the position labeled by the angle θ is obtained directly from Eq. (4):

$$j(\theta, t) = D \sum_{m=-\infty}^{\infty} \sum_{n=1}^{\infty} \frac{\cos(m\theta)F_{mn}(r_0)k_{mn}^2 e^{-k_{mn}^2 D t}}{C_{mn}} \quad (10)$$

The expressions for the density and hitting distribution can be compared with those of the corresponding unbounded system ($b = \infty$, indicated by an asterisk)⁴⁴:

$$c^*(r, \theta, t) = \sum_{m=-\infty}^{\infty} \frac{\cos(m\theta)}{2\pi} \int_0^{\infty} \frac{F_m(r)F_m(r_0)k e^{-k^2 D t} dk}{J_m^2(ka) + Y_m^2(ka)} \quad (11)$$

and

$$j^*(\theta, t) = \frac{D}{\pi^2} \sum_{m=-\infty}^{\infty} \cos(m\theta) \int_0^{\infty} \frac{F_m(r_0)k e^{-k^2 D t} dk}{J_m^2(ka) + Y_m^2(ka)} \quad (12)$$

where F_m is

$$F_m(r) = Y_m(kr)J_m(ka) - J_m(kr)Y_m(ka) \quad (13)$$

As shown in⁴⁸, the eventual hitting angle distribution $\tilde{J}(\theta) = \int_0^{\infty} j(\theta, t) dt$ for the bounded case is given by

$$\tilde{J}(\theta) = \frac{1}{2\pi} \left[1 + 2 \sum_{m=1}^{\infty} c_m \cos(m\theta) \right] \quad (14)$$

with

$$c_m = \frac{r_0^{2m} + b^{2m}}{a^{2m} + b^{2m}} \left(\frac{a}{r_0} \right)^m \quad (15)$$

which reduces to the unbounded case (see e.g.¹⁶) in the limit $b \rightarrow \infty$

$$\tilde{j}^*(\theta) = \frac{1}{2\pi} \frac{1 - a^2/r_0^2}{1 - (2a/r_0)\cos\theta + a^2/r_0^2}, \quad (16)$$

The distribution (14) is normalized, $\int_{-\pi}^{\pi} d\theta \tilde{j}(\theta) = 1$, which is consistent with the certainty of (eventually) hitting the target in two dimensions (Pólya's recurrence theorem^{16,53}).

III. DIFFUSIVE ECHO IN 2D

For all values of θ and $r_0 \in [a, b]$, the instantaneous local target flux $j(\theta, t)$ initially increases from zero, then passes through one or two maxima, before decreasing exponentially to zero. The short-time evolution of $j(\theta, t)$ is similar to $j^*(\theta, t)$, but the bounded system may display two maxima at intermediate times, an effect referred to as a 'diffusive echo' in the following.

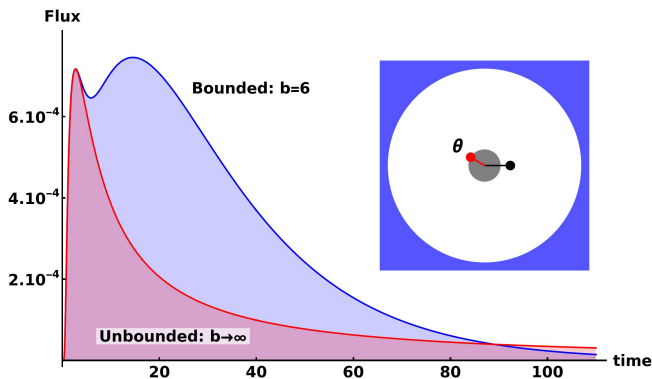


FIG. 2. Manifestation of a diffusive echo. Time evolution of the hitting angle distribution $j(\theta, t)$ of a bounded system ($b = 6$, upper curve) compared with $j^*(\theta, t)$ for an unbounded system ($b = \infty$, lower curve). In both cases: $a = 1$, $r_0 = 1.6$ and $\theta = 5\pi/6$.

An example of a double maximum is shown in Fig. 2 for $a = 1$, $b = 6$, $r_0 = 1.6$, and for a particular hitting angle $\theta = 5\pi/6$. The unbounded distribution is also shown for comparison. As expected, the instantaneous flux to any target position the targeted position is higher for a bounded system until about $t \approx 90$ (2.5 in units of b^2/D) since, in the unbounded case, part of the flux leaks into the external region $r > b$. For times greater than this, the opposite trend occurs. The slow decrease in the unbounded case is due to the possibility for the diffusing particle to return to the target after a long time away from it, whereas in the bounded case the particle is consumed rapidly.

While the first peak of $j(\theta, t)$ is common to the bounded and unbounded cases, the presence of the confining boundary leads to a second peak in the target local flux. A series of such curves for different values of the initial position between $a < r_0 < b$ is shown in Fig. 3.

We observe a switching between two diffusion regimes. For r_0 far from the target and close to the reflecting boundary, $j(\theta, t)$ is totally different from the unbounded case and is

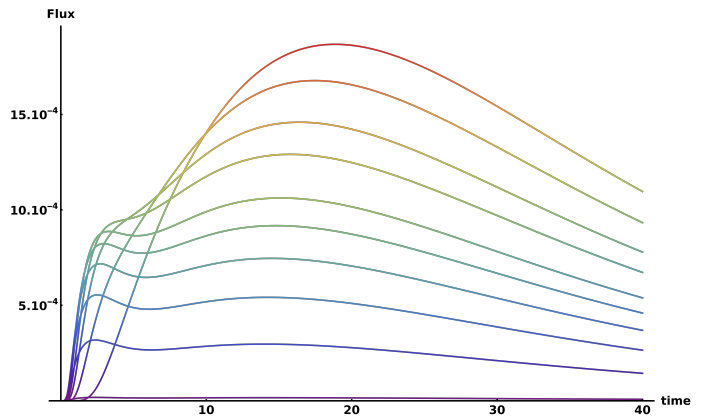


FIG. 3. Flux $j(\theta, t)$ at a hitting angle $\theta = 5\pi/6$ for various starting points. From top to bottom $r_0 = 6, 3.6, 2.8, 2.4, 2, 1.8, 1.6, 1.4, 1.2, 1.01$. The confinement is $b = 6$.

strongly influenced by the confinement. On the other hand, for r_0 far enough from the external boundary, the latter is not felt at short times and the flux to the target is controlled by "direct" diffusion. At later times, an indirect flux, due to reflection by the external boundary, is dominant. For intermediate values of r_0 , these two regimes superpose and a double maximum in $j(\theta, t)$ may appear.

An interesting consequence of the double maxima of Figs. 2 and 3 is that the flux is sustained at a high value for a much longer time than in the unbounded case. This can be quantified by comparing the length of time during which the hitting distribution is higher than a specific value, for both the bounded and unbounded cases. This specific threshold value may be chosen as the value of the local minimum of $j(\theta, t)$, i.e. between its two consecutive maxima. For example, for $r_0 = 1.6$, one gets a flux of $6.5 \cdot 10^{-4}$ (in units of D/a^2) as shown in Fig. 2. For this flux value, the width of the distribution peak of the bounded system is more than 8.5 times the width of the unbounded distribution. For $r_0 = 2$, the difference is even larger: the bounded distribution peak is more than 15 times larger than the unbounded distribution.

As already underlined, the confining boundary leads to a redistribution of the hitting probability in the course of time. The time integral of $j(\theta, t)$ can therefore approach its infinite time value long before the time integral of $j^*(\theta, t)$. In other words, the probability to reach a specific target can be much more concentrated for a confined system than for an unbounded one, providing the starting position r_0 is well chosen. The diffusive echo phenomenon is thus not merely a mathematical curiosity, but may be exploited to significantly enhance the efficiency of a passive diffusive search. More specifically, for example, it may play a role in determining *where* a therapeutic molecule should be injected in a cell in order to more efficiently reach a targeted zone in the inner core of the cell. For a core of one-sixth of the cell size, $b = 6a$, the ideal starting location is close to $r_0 \simeq 2a$ for a target located at the angle $\theta = 5\pi/6$, i.e. on the opposite side of the core from the departure point.

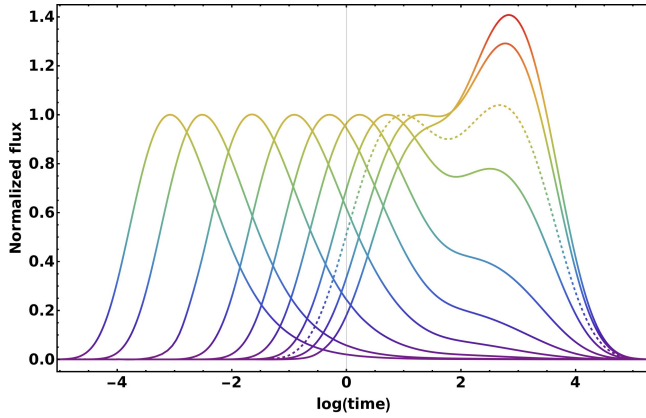


FIG. 4. Normalized flux $j(\theta, t)/j_{\max}$ at different hitting angles θ from the same starting point $r_0 = 1.6$. From left to right $\theta = 0, 0.4, 0.8, 1.2, 1.6, 2, 2.4, 2.8, \pi$. The case $\theta = 5\pi/6$ of Fig. 2 is also shown for comparison (dashed line). The confinement is $b = 6$.

The dependence of the diffusive echo on θ is subtle (see Fig. 4). For small and large θ , only one maximum is present, i.e. there is no diffusive echo. The explanation relies on the sink effect of the absorbing inner circle. For small values of θ , the direct flux to the targeted point specified by θ is not impeded by the remaining part of the absorbing inner circle. As a consequence, the direct flux to the target is sufficiently high so that it is not overcome by the subsequent indirect flux from the outer boundary. On the other hand, for a targeted point on the opposite side of the inner circle ($\theta \simeq \pi$), the absorbing inner boundary plays the role of a sink that prevents direct diffusion towards the targeted point, allowing the confinement-controlled diffusion to dominate. For intermediate θ values, these two processes compete and a double maximum in $j(\theta, t)$ may appear. On the right hand side of Fig. 4, one clearly sees the gradual build-up of a second, reflection-induced flux maximum. For $\theta = 5\pi/6$ (dashed line in Fig. 4), the diffusive echo is more apparent since the two maxima have a similar amplitude.

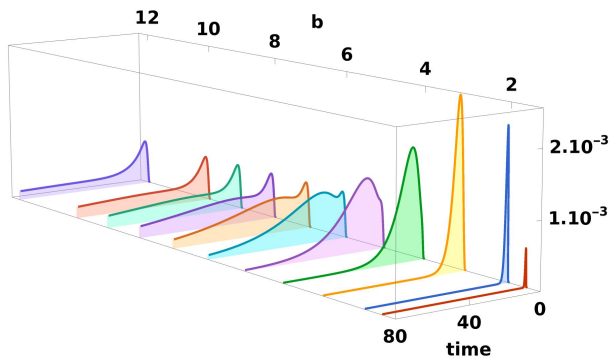


FIG. 5. Flux $j(\theta, t)$ at a hitting angle $\theta = 5\pi/6$ from the same starting point $r_0 = 1.6$ but for various values of the confining parameter b . From bottom right to top left: $b = 1.6$ (coinciding with the starting point), 2, 3, 4, 5, 6, 7, 8, 9, 10, 12.

The dependence of the diffusive echo on the degree of confinement may be explained similarly (see Fig. 5 and 6). For small values of b , the reflecting boundary guides the diffusing particle around the central circle. Due to the proximity of the absorbing inner boundary, there is almost no direct diffusion toward the specific targeted θ -point, particularly if it is on the opposite side of the starting point. All possible 'direct' trajectories are indeed too close to the absorbing central zone and only 'indirect' trajectories can survive and contribute to the flux on the targeted point, especially when the starting point is close to the inner absorbing circle (i.e. for small values of r_0). For larger values of b , i.e. for a weaker confinement, this indirect flux decreases since many of the indirect trajectories seep from the target area and are no longer focused on it. The intensity of the direct flux becomes comparable with the reflected one, enabling a diffusive echo on the targeted point since these two fluxes are time shifted. Finally, for very weak confinement ($b \gg a$), the reflected flux is tenuous and one recovers the unbounded behavior.

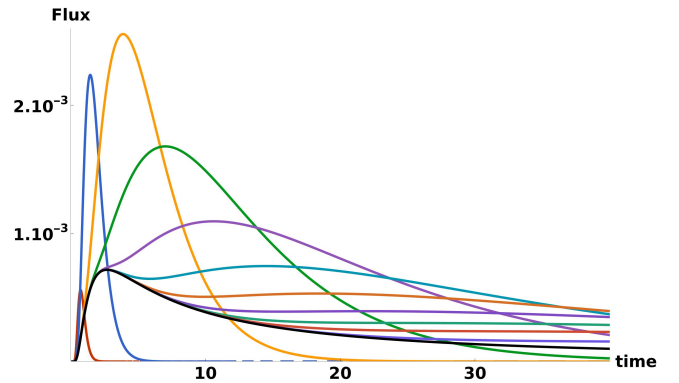


FIG. 6. Same curves as in Fig. 5 (with the same color code), but regrouped in a single 2D graphic. The additional black curve corresponds to the unbounded case ($b \rightarrow \infty$).

For very strong confinement, we observe a narrow distribution of the flux whose maximum occurs at a much shorter time than in the unbounded case (see Fig. 6, the first two curves on the left). This effect strongly depends on the starting position r_0 as expected from a simple explanation in terms of survival of trajectories. Indeed, for r_0 very close to the confining boundary, almost all the trajectories are focused initially towards the absorbing central zone. For highly confined systems (small b), these trajectories cannot escape and are absorbed due to the lack of space. As a consequence, the average time needed to reach a specific targeted point is reduced since almost no trajectories can survive for a long time. On the contrary, as soon as r_0 is no longer close to b , some trajectories may escape through the back side (or on the left/right sides) during the first instants of the diffusion process and then be guided by the confining boundary, leading to a higher contribution to the flux on a distant point. Among all trajectories, the weight of the longest ones increase in the distribution of the hitting times: the flux maximum is thus higher than in the unbounded case, and occurs at a later time. Then, as explained

above, for higher values of b , the space available to the diffusing particle becomes sufficient to allow for longer and longer survival times, and the hitting times distribution broadens and flattens. There is therefore an optimum value of the confining parameter b for which the flux on a specific targeted point is the highest (this optimal b value being close to 3 for $r_0 = 1.6$ as shown in Fig. 6).

We present some examples of the joint distribution of the hitting angle and hitting time for a system with $a = 1, b = 6$ for different values of r_0 in Fig. 7. The contour lines help to clarify the role of hitting angle in the set up of diffusive echo for small starting positions, and its gradual disappearance for higher r_0 values.

For completeness, Fig. 8 shows heat maps obtained from brownian dynamics simulations for a system with $a = 1, b = 4$ for various values of r_0 . Each point shows the hitting angle and hitting time of a single trajectory. These results are also compared with the theoretical values of three typical first passage times to the whole inner absorbing sphere: the most probable t_{prob} , mean $\langle t \rangle$ and median t_{median} first passage times (see the Appendix B).

IV. DIFFUSIVE ECHO IN 3D

For unbounded diffusive search, it is well known that the dimensionality d of the system plays a major role. The diffusive exploration is compact for $d \leq 2$ whereas it is only transient for $d > 2$ (Pólya's recurrence theorem^{16,53}). For $d = 3$, for example, the fraction of particles that never reaches the inner absorbing sphere at $r = a$ is equal to $1 - a/r_0$. However, if a reflecting barrier is present, these particles are not lost and eventually contribute to the flux on $r = a$, leading to non-intuitive results when the barrier is shifted to infinity⁴⁸.

The issue of the presence of a diffusive echo in $d > 2$ systems is also of interest since one expects seeing two competing effects at stake: the reflection from the external spherical barrier which focuses the diffusive flux toward the target, and the dispersion of the particles in a volume that becomes larger and larger as d increases.

For simplicity we consider the model shown in Fig. 1 where a spherical absorbing surface of radius a is contained within a spherically symmetric reflecting wall of radius b . As for the 2D case, our aim is to compute the joint probability that a diffusing particle hits a specific position on the perfectly absorbing central surface.

Due to the spherical symmetry of the system, only one angle θ is sufficient to label the targeted position with respect to the starting position, and the diffusion equation can be reduced to a simpler equation, similar to the one in 2D.

As a result, the expression of the flux in more than 2 dimensions is similar to the expression Eq. (10) of the 2D flux. For example, in 3D, the main differences are that the $\cos(\theta)$ term is replaced by a Legendre polynomial in $\cos \theta$ and the Bessel functions are replaced by spherical Bessel functions.

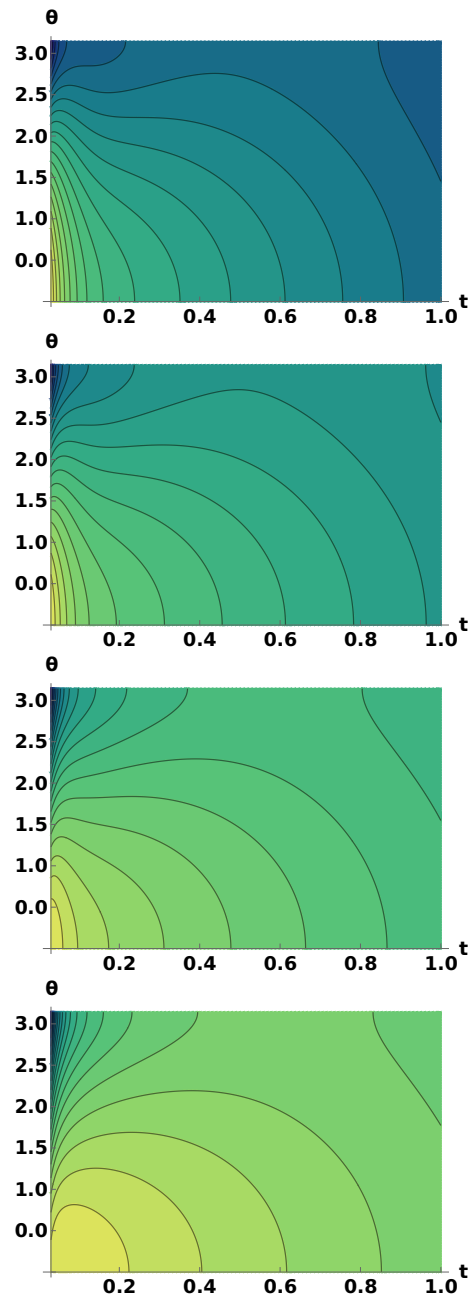


FIG. 7. Heat maps of the (log of the) joint distribution of the hitting angle θ and hitting time t (expressed in units of b^2/D) for a particle starting its diffusive trajectory at a distance $r_0 = 1.6, 2.6, 3.6, 4.6$, top to bottom, in an annulus with $a = 1, b = 6$.

The explicit expression for the flux is

$$j_{3D}(\theta, t) = 2aD \sum_{m=0}^{+\infty} \left(m + \frac{1}{2}\right) P_m(\cos \theta) \times \sum_{n=1}^{+\infty} \frac{k_{mn}^3 f_{mn}(r_0) e^{-Dk_{mn}^2 t}}{c_{mn}} \quad (17)$$

(see the Appendix C for more details).

The diffusive echo is thus also expected for $d > 2$. Fig.

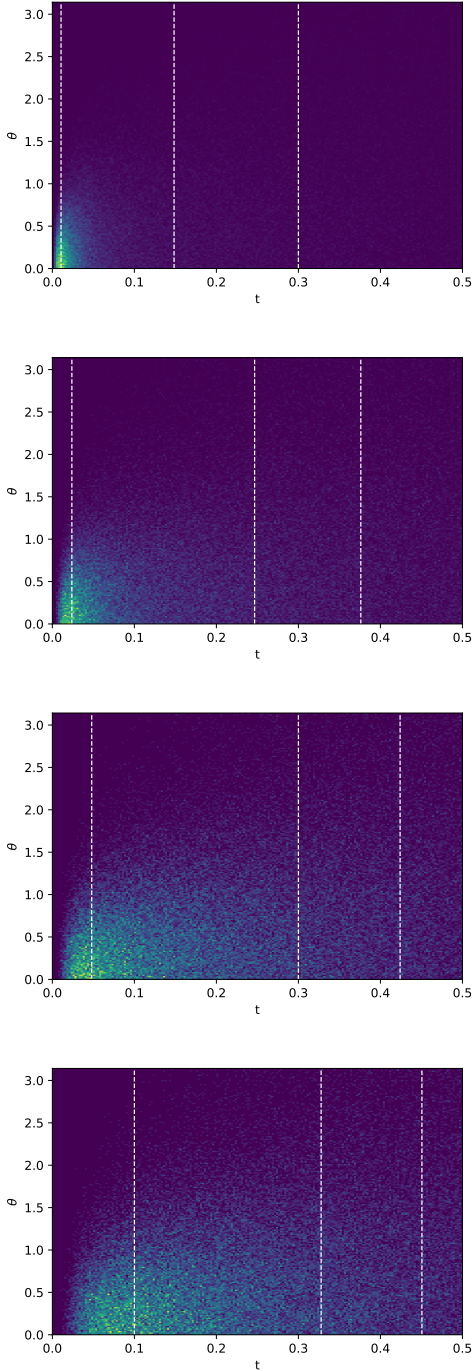


FIG. 8. Heat maps of the joint distribution of the hitting angle θ and hitting time t (expressed in units of b^2/D) for a particle starting its diffusive trajectory at a distance r_0 . The geometry is defined by $a = 1, b = 4$ and $r_0 = 2, 2.5, 3, 3.5$, top to bottom. The dashed vertical lines show the most probable, median and mean first passage times from left to right, respectively.

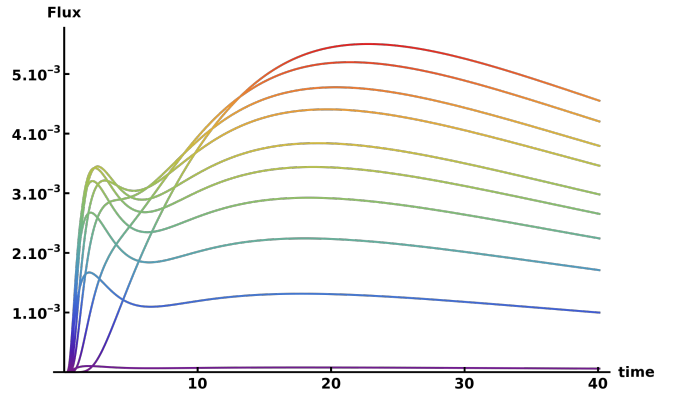


FIG. 9. 3D flux $j_{3D}(\theta, t)$ at a hitting angle $\theta = \frac{5\pi}{6} \simeq 2.6$ for various starting points. From top to bottom $r_0 = 6, 3.6, 2.8, 2.4, 2, 1.8, 1.6, 1.4, 1.2, 1.01$. The confinement is $b = 6$.

(9) and (10) show how the instantaneous local target flux can present a clear double maximum for a range of starting position r_0 , targeted position angle θ and reflecting wall radius b .

The diffusive echo is even more pronounced than in 2D, with a more profound dip between the two maxima. The more intense dispersion (in a larger volume) is offset by increased focusing effect of the external spherical barrier.

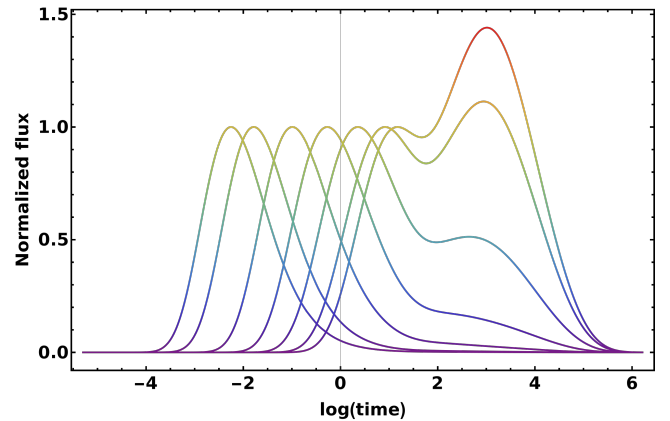


FIG. 10. 3D normalized flux $j_{3D}(\theta, t) / j_{\text{first max}}(\theta, t)$ at different hitting angles θ from the same starting point $r_0 = 1.6$. From left to right $\theta = 0, \frac{\pi}{6}, \frac{\pi}{3}, \frac{\pi}{2}, \frac{2\pi}{3}, \frac{5\pi}{6}, \pi$. The confinement is $b = 6$.

V. ONE DIMENSION AND DISCUSSION

The diffusive echo phenomenon is almost imperceptible for one-dimensional ($d = 1$) systems^{22,23}. As recalled in the Appendix A, for a diffusive process on a segment with reflecting ($r = b$) and absorbing ($r = a$) boundaries, the expression of the instantaneous flux to the absorbing point is given by

$$j_{1D}(t) = \frac{2D}{b-a} \sum_{n=1}^{\infty} \sin[k_{0n}(r_0 - a)] k_{0n} e^{-Dk_{0n}^2 t} \quad (18)$$

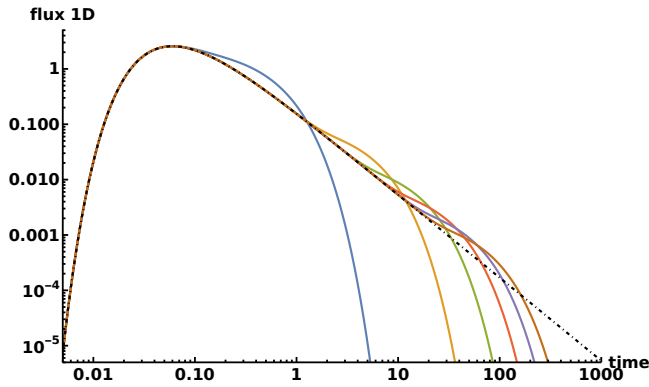


FIG. 11. 1D time dependent flux on the target, for $a = 1$ and various values of the confining parameter, $b = 2, 4, 6, 8, 10, 12$, from left to right. The dot-dashed line is for the unbounded case $b = \infty$. The starting point is $r_0 = 1.6$ for all curves.

with $k_{0n} = \pi(n - 1/2)/(b - a)$.

Initially, the flux is null, $j_{1D}(0) = 0$, whatever the starting position. It then increases, reaches a maximum and decays exponentially to zero. The exponential time decrease is controlled by the square of the first root, k_{01}^2 , which is nine times smaller than the square of the other roots. The first term in (18) is thus dominant at mid and long term, and no other term can overcome it to create a true echo. The presence of the reflecting boundary is visible only at very long time, in the tail of the flux, where a shoulder is scarcely observable on a log-log scale (see Fig. 11 and ^{22,23}).

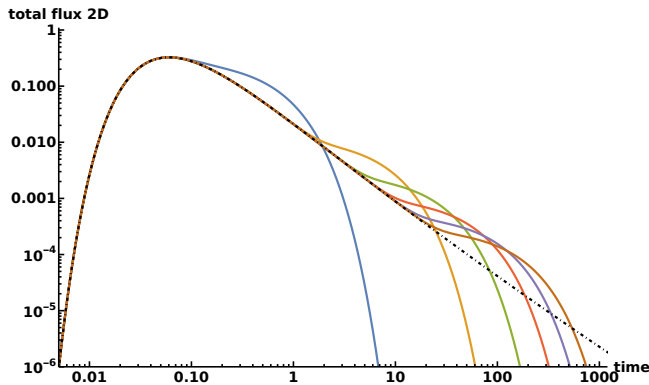


FIG. 12. Same as Fig. 11 except 2D

For an echo to appear, the presence of an additional variable, like the angle θ in the 2D and 3D cases described above, appears to be crucial. Depending on its value, this variable may lead to negative terms in the expression of the flux (for example when $\theta \in [\pi/2, \pi]$ for the terms labelled by $m = 1$). Similarly to what happens for destructive and constructive interference, one observes a modulation of the flux in the course of time for certain angles.

As one might expect, integrating the flux over the angle θ (see the Appendixes B and C for the resulting expressions) eliminates the echo and one is left with a shoulder on a log-log plot of the flux versus time, as seen in Fig. 12 and Fig.

13.

An examination of the expressions of the fluxes in 2D, Eq. (10), and 3D, Eq. (17), shows that only a few terms in the sums are needed to account for the echo effect. In 3D for example it suffices to consider the first four terms $n = 1, 2$ and $m = 0, 1$ in Eq. (17) to get the double maximum in the flux (see Fig. 14). With the first sixteen terms (i.e. n from 1 to 4, and m from 0 to 3), one obtains a curve which is almost indistinguishable from the full curve obtained for $n \rightarrow \infty$ and $m \rightarrow \infty$.

The roots k_{mn} that intervene in the flux expressions Eq. (10) and Eq. (17) are approximately independent of m :

$$k_{mn} \simeq \frac{\pi(n - \frac{1}{2})}{b - a}, \quad \forall m \quad (19)$$

As a consequence, for each value of n , all the terms $e^{-Dk_{mn}^2 t}$ evolve in a similar way and can be regrouped. The factors $\cos(m\theta)$ in 2D and $P_m(\cos\theta)$ in 3D may be negative depending on the value of θ , creating the conditions for a bell-shape curve for each packet of terms labelled by the same value of n . The first packet ($n = 1$) corresponds to the flux reflected from the external confining boundary ('indirect'), whereas the second one corresponds to the 'direct' diffusive process towards the target. See Fig. 14. The intensity of these different contributions to the flux is governed by r_0 and b .

In summary, and contrary to the acoustic case, a 'true' diffusive echo (i.e. with two well identified maxima in the time-dependent local flux) cannot exist for one dimensional diffusive processes. Rather counter-intuitively, however, the diffusive echo phenomenon intensifies as the dimension increases. Due to the echo, the interval of peak flux can be largely extended in time, showing the relevance of the phenomenon for enhancing the search efficiency in a confined environment.

Although quite simple, the geometry considered here allows one to grasp the essence of the phenomenon. Further research could explore other, more constrained geometries for which multiple diffusive echoes might appear. In particular, the optimum geometry for observing the strongest echo is an open question (as well as the maximum number of observable echoes). The diffusive echo induced by moving obstacles is also worth considering, given its relevance for real diffusive

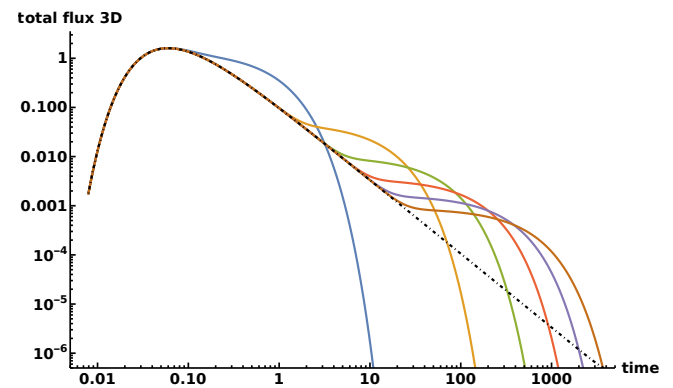


FIG. 13. Same as Fig. 11 except 3D

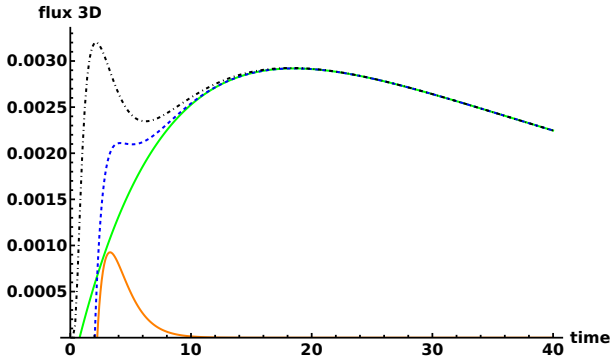


FIG. 14. The flux $j_{3D}(\theta, t)$ on the spherical absorber at a hitting angle $\theta = 5\pi/6$. The starting point is $r_0 = 1.6$ and the reflecting wall is at $b = 6$. The two continuous lines correspond to the partial sums $n = 1; m = 0, 1$ ('indirect') and $n = 2; m = 0, 1$ ('direct'). The dashed line corresponds to their sum, while the dot-dashed line is the full expression of the flux.

processes. In a similar vein, an effort could be made to determine the role of the absorbing central area in the manifestation of the diffusive echo.

These results could shed light on biological diffusive processes such as those that govern the (passive) search for a specific target in a living, confined environment where traps or lethal zones may impede the search.

Acknowledgements. We thank Denis Grebenkov for informing us about his recent work that presents related expressions as well as other references.

APPENDIXES

Here we detail the solution of the time-dependent diffusion equations in 1D, 2D and 3D that are necessary to obtain the time dependent hitting angle distribution.

Appendix A: One dimension

The (Green's function of the) concentration $c(r, t)$, $a \leq r \leq b$, obeys the following diffusion equation

$$\frac{\partial c}{\partial t'} - \frac{\partial^2 c}{\partial r'^2} = \delta(r' - r'_0) \delta(t') \quad (\text{A1})$$

with the boundary condition $c(a, t) = 0$, $\partial c / \partial r|_{r=b} = 0$ in terms of dimensionless variables $r' = r/a$ and $t' = Dt/a^2$. In the following we drop the primes for simplicity.

This one dimensional problem can be solved simply, but here we use a slightly more complicated method that parallels the treatment of the other dimensions.

Introducing the Laplace transform $\hat{f}(s) = \int_0^\infty dt e^{-st} c(r, t)$, one obtains the following differential equation

$$\frac{d^2 \hat{f}}{dx^2} - \hat{f} = -\frac{\delta(x - x_0)}{\sqrt{s}} \quad (\text{A2})$$

where we have introduced the reduced variable $x = r\sqrt{s}$.

The boundary conditions $\hat{f}(x_a) = 0$ and $\frac{d\hat{f}}{dx}(x_b) = 0$ imply that the global solution can be written as the combination of interior and exterior solutions

$$\begin{cases} \hat{f}_<(x) &= A \sinh(x - x_a), x < x_0 \\ \hat{f}_>(x) &= B \cosh(x_b - x), x > x_0 \end{cases} \quad (\text{A3})$$

Then, by continuity of \hat{f} and integration of (2) across the discontinuity of $d\hat{f}/dx$ in x_0 , one finally gets

$$\hat{f}(x) = \frac{\sinh(x_< - x_a) \cosh(x_b - x_>)}{\sqrt{s} \cosh(x_b - x_a)} \quad (\text{A4})$$

with $x_< = \min(x, x_0)$ and $x_> = \max(x, x_0)$.

The inverse Laplace transform and residue theorem provide the global solution

$$\begin{aligned} c(r, \theta, t) &= \frac{1}{2\pi i} \int_{\gamma-i\infty}^{\gamma+i\infty} ds e^{Dst} \hat{f}(x) \\ &= \sum_n \text{Res} \left[e^{Dst} \hat{f}(x) \right] \end{aligned} \quad (\text{A5})$$

where the sum of the residues is over the singularities of \hat{f} , i.e. over the roots s_n of the auxiliary equation

$$g(s) = \cosh(\sqrt{s}(b-a)) = 0 \quad (\text{A6})$$

which are

$$\sqrt{s_n} = -ik_{0n}, n \in \mathbb{N}^* \quad (\text{A7})$$

with

$$k_{0n} = \frac{\pi(n - \frac{1}{2})}{b-a} \quad (\text{A8})$$

The term $g'(s_n)$ needed to calculate the residue is

$$g'(s_n) = \frac{(b-a)}{2k_{0n}} (-1)^{n+1} \quad (\text{A9})$$

and one finally obtains

$$c(r, t) = \frac{2}{b-a} \sum_{n=1}^{\infty} e^{-Dk_{0n}^2 t} \sin[k_{0n}(r-a)] \sin[k_{0n}(r_0-a)] \quad (\text{A10})$$

where the completeness relation of the basis functions $\sin[k_{0n}(r_0-a)]$ reads

$$\begin{aligned} c(r, 0) &= \frac{2}{b-a} \sum_{n=1}^{\infty} \sin[k_{0n}(r-a)] \sin[k_{0n}(r_0-a)] \\ &= \delta(r - r_0) \end{aligned} \quad (\text{A11})$$

The instantaneous flux in $r = a$ is

$$\begin{aligned} j_{1D}(t) &= D \frac{\partial c}{\partial r} \Big|_a \\ &= \frac{2D}{b-a} \sum_{n=1}^{\infty} \sin[k_{0n}(r_0-a)] k_{0n} e^{-Dk_{0n}^2 t} \end{aligned} \quad (\text{A12})$$

and the cumulative hitting probability $J_{1D}(t) = \int_0^t j_{1D}(t') dt'$ at time t is

$$J_{1D}(t) = \frac{2}{b-a} \sum_{n=1}^{\infty} \left(1 - e^{-Dk_{0n}^2 t}\right) \frac{\sin[k_{0n}(r_0 - a)]}{k_{0n}} \quad (\text{A13})$$

which converges monotonically to 1 when $t \rightarrow \infty$.

In the limit of an infinitely distant confining wall, $b \rightarrow \infty$, we recover the usual unbounded expressions

$$c^*(r, t) = \frac{1}{2\sqrt{\pi Dt}} \left(e^{-\frac{(r-r_0)^2}{4Dt}} - e^{-\frac{(2a-r-r_0)^2}{4Dt}} \right) \quad (\text{A14})$$

and

$$J_{1D}^*(t) = \int_0^t j^*(t') dt' = 1 - \operatorname{erf}\left(\frac{r_0 - a}{2\sqrt{Dt}}\right) \quad (\text{A15})$$

Appendix B: Two dimensions

The concentration $c(r, \theta, t)$, $a \leq r \leq b$, $-\pi \leq \theta \leq \pi$, where r is the radial distance from the center of the target and θ is the azimuthal angle, obeys the following diffusion equation

$$\frac{\partial c}{\partial t} - \frac{\partial^2 c}{\partial r^2} - \frac{1}{r} \frac{\partial c}{\partial r} - \frac{1}{r^2} \frac{\partial^2 c}{\partial \theta^2} = \frac{\delta(r' - r'_0) \delta(\theta) \delta(t)}{r'_0}, \quad (\text{B1})$$

with the boundary conditions $c(a, \theta, t) = 0$, $\partial c / \partial r|_{r=b} = 0$ in terms of dimensionless variables $r' = r/a$ and $t' = Dt/a^2$. In the following we drop the primes for simplicity.

Since the angle dependence is symmetric in θ , the solution is necessarily of the form

$$c(r, \theta, t) = \sum_{k=-\infty}^{+\infty} \cos(k\theta) f_k(r, t) \quad (\text{B2})$$

Multiplying both sides of (B1) by $\cos(m\theta)$ and integrating over θ leads to

$$\frac{\partial f_m}{\partial t} - \frac{\partial^2 f_m}{\partial r^2} - \frac{1}{r} \frac{\partial f_m}{\partial r} + \frac{m^2}{r^2} f_m = \frac{\delta(r - r_0) \delta(t)}{2\pi r_0} \quad (\text{B3})$$

since $\int_{-\pi}^{+\pi} d\theta \cos(k\theta) \cos(m\theta) = \pi \delta_{k,|m|}$ and $f_{-m} = f_m$. Introducing the Laplace transform $\widehat{f}_m(x) = \int_0^\infty dt e^{-st} f_m(x, t)$, one finally obtains the following well-known differential equation

$$\frac{d^2 \widehat{f}_m}{dx^2} + \frac{1}{x} \frac{d\widehat{f}_m}{dx} - \left(1 + \frac{m^2}{x^2}\right) \widehat{f}_m = -\frac{\delta(x - x_0)}{2\pi x_0} \quad (\text{B4})$$

where the reduced variable $x = r\sqrt{s}$ has been introduced.

The boundary conditions

$$\widehat{f}_m(x_a) = 0 \quad \text{and} \quad \frac{\partial \widehat{f}_m}{\partial x}(x_b) = 0, \quad (\text{B5})$$

corresponding to absorption at $r = a$ and reflection at $r = b$ respectively, imply that the global solution can be written as

the combination of interior and exterior solutions:

$$\begin{aligned} \widehat{f}_{m<}(x) &= A_m (I_m(x) K_m(x_a) - K_m(x) I_m(x_a)) \\ \widehat{f}_{m>}(x) &= B_m (I_m(x) K'_m(x_b) - K_m(x) I'_m(x_b)) \end{aligned} \quad (\text{B6})$$

in terms of $I_m(x)$ and $K_m(x)$, the modified Bessel functions of the first and second kind of order m .

Then, by continuity of \widehat{f}_m and integration of (B4) across the discontinuity in x_0 , one finally gets

$$\widehat{f}_m(x) = \frac{1}{2\pi} \frac{(I'_{mb} K_{m>} - K'_{mb} I_{m>}) (I_{m<} K_{ma} - K_{m<} I_{ma})}{I'_{mb} K_{ma} - K'_{mb} I_{ma}} \quad (\text{B7})$$

with $x_{<} = \min(x, x_0)$ and $x_{>} = \max(x, x_0)$, and where, for example, I'_{mb} and $K_{m>}$ stand for $\frac{\partial I_m}{\partial x}(x_b)$ and $K_m(x_{>})$, respectively.

The inverse Laplace transform and residue theorem provide the global solution in the time domain in terms of dimensional variables

$$\begin{aligned} c(r, \theta, t) &= \sum_{m=-\infty}^{+\infty} \frac{\cos(m(\theta - \theta_0))}{2\pi i} \int_{\gamma-i\infty}^{\gamma+i\infty} ds e^{Dst} \widehat{f}_m(x) \\ &= \sum_{m=-\infty}^{+\infty} \cos(m(\theta - \theta_0)) \sum_n \operatorname{Res} \left[e^{Dst} \widehat{f}_m(x) \right] \end{aligned} \quad (\text{B8})$$

where the sum of the residues is over the singularities of \widehat{f}_m , i.e. over the roots s_n of the auxiliary equation

$$g(s) = I'_m(qb) K_m(qa) - K'_m(qb) I_m(qa) = 0 \quad (\text{B9})$$

where $q = \sqrt{s}$.

The term $g'(s_n)$ appearing in the residue is

$$\begin{aligned} g'(s_n) &= \frac{b}{2q_n} (I''_{mb} K_{ma} - K''_{mb} I_{ma}) \\ &\quad + \frac{a}{2q_n} (I'_{mb} K'_{ma} - K'_{mb} I'_{ma}) \end{aligned} \quad (\text{B10})$$

(in shorthand notation here, but evaluated in $s = s_n$), which can be simplified thanks to (B9) as

$$\begin{aligned} g'(s_n) &= \frac{b}{2q_n} \frac{I_{ma}}{I'_{mb}} (I''_{mb} K'_{mb} - K''_{mb} I'_{mb}) \\ &\quad + \frac{a}{2q_n} \frac{I'_{mb}}{I_{ma}} (I_{ma} K'_{ma} - K_{ma} I'_{ma}) \end{aligned} \quad (\text{B11})$$

Then, using the Bessel identities

$$I_m(q_n a) K'_m(q_n a) - K_m(q_n a) I'_m(q_n a) = -\frac{1}{q_n a} \quad (\text{B12})$$

$$I''_m(q_n b) K'_m(q_n b) - K''_m(q_n b) I'_m(q_n b) = -\frac{(q_n b)^2 + m^2}{(q_n b)^3} \quad (\text{B13})$$

the function $g'(s_n)$ reads

$$g'(s_n) = -\frac{1}{2q_n^2} \left(\frac{I'_{mb}}{I_{ma}} + \frac{I_{ma}}{I'_{mb}} \left(1 + \left(\frac{m}{q_n b} \right)^2 \right) \right) \quad (\text{B14})$$

Replacing in (B7) K'_{mb} by $I'_{mb}K_{ma}/I_{ma}$ thanks to (B9), one obtains

$$c(r, \theta, t) = \sum_{m=-\infty}^{+\infty} \frac{\cos(m\theta)}{\pi} \sum_n e^{Dq_n^2 t} q_n^2 \times \frac{(K_{m>I_{ma}} - I_{m>K_{ma}})(K_{m<I_{ma}} - I_{m<K_{ma}})}{1 + \left(\frac{I_{ma}}{I'_{mb}} \right)^2 \left(1 + \left(\frac{m}{q_n b} \right)^2 \right)} \quad (\text{B15})$$

where the product $(K_{m>I_{ma}} - I_{m>K_{ma}})(K_{m<I_{ma}} - I_{m<K_{ma}})$ may also be written as $(K_{mr}I_{ma} - I_{mr}K_{ma})(K_{mr_0}I_{ma} - I_{mr_0}K_{ma})$ in terms of the variables r and r_0 .

Since the solutions $q_n = \sqrt{s_n}$ of $g(s) = 0$ are purely imaginary: $q_n = ik_n$, with $k_n \in \mathbb{R}$, one can switch to the Bessel functions of the first and second kind, J_m and Y_m , using the relations

$$\begin{aligned} I_m(ik_n u) &= i^m J_m(k_n u) \\ I'_m(ik_n u) &= i^{m-1} J'_m(k_n u) \\ K_m(ik_n u) &= \frac{\pi}{2} (-i)^m [-iJ_m(k_n u) - Y_m(k_n u)] \end{aligned} \quad (\text{B16})$$

for m integer in the last expression.

The final solution gives back the expression (6):

$$c(r, \theta, t) = \sum_{m=-\infty}^{+\infty} \frac{\pi}{2} \cos(m\theta) \times \sum_{n=1}^{+\infty} e^{-Dk_{mn}^2 t} k_{mn}^2 \frac{F_{mn}(r) F_{mn}(r_0)}{C_{mn}} \quad (\text{B17})$$

with the coefficients C_{mn} given by

$$C_{mn} = 2 \left[\left(\frac{J_m(k_{mn}a)}{J'_m(k_{mn}b)} \right)^2 \left(1 - \left(\frac{m}{k_{mn}b} \right)^2 \right) - 1 \right] \quad (\text{B18})$$

with

$$F_{mn}(r) = Y_m(k_{mn}r)J_m(k_{mn}a) - J_m(k_{mn}r)Y_m(k_{mn}a) \quad (\text{B19})$$

where k_{mn} is the n^{th} solution of the m^{th} auxiliary equation

$$Y'_m(kb)J_m(ka) - J'_m(kb)Y_m(ka) = 0 \quad (\text{B20})$$

The completeness relation of the basis functions $k_{mn}F_{mn}(r)/\sqrt{C_{mn}}$, reads (whatever the value of m)

$$\sum_{n=1}^{+\infty} \pi^2 k_{mn}^2 \frac{F_{mn}(r) F_{mn}(r_0)}{C_{mn}} = \frac{\delta(r-r_0)}{r_0} \quad (\text{B21})$$

for any value of m , since $\sum_{m=-\infty}^{+\infty} \cos(m\theta) = 2\pi\delta(\theta)$ in the $c(r, \theta, 0)$ expression.

The instantaneous flux at a specific point ($r = a, \theta$) of the absorbing inner boundary is

$$j(\theta, t) = aD \frac{\partial c}{\partial r} \Big|_a = D \sum_{m=-\infty}^{+\infty} \sum_{n=1}^{+\infty} \frac{\cos(m\theta) F_{mn}(r_0) k_{mn}^2 e^{-Dk_{mn}^2 t}}{C_{mn}} \quad (\text{B22})$$

since $\frac{\partial F_{mn}}{\partial r}(a) = 2/\pi a$ thanks to the Bessel identity (B12).

The cumulative hitting probability $J(\theta, t) = \int_0^t j(\theta, t') dt'$ in θ at time t is

$$J(\theta, t) = \sum_{m=-\infty}^{+\infty} \sum_{n=1}^{+\infty} \frac{\cos(m\theta) F_{mn}(r_0) (1 - e^{-Dk_{mn}^2 t})}{C_{mn}} \quad (\text{B23})$$

whose integral over θ

$$\int_{-\pi}^{\pi} J(\theta, t) d\theta = 2\pi \sum_{n=1}^{+\infty} \frac{F_{0n}(r_0) (1 - e^{-Dk_{0n}^2 t})}{C_{0n}} \quad (\text{B24})$$

converges monotonically to 1 for $t \rightarrow \infty$ (whatever the value of r_0).

The total flux to the inner absorbing circle can also be computed:

$$j_{tot}(t) = \int_{-\pi}^{\pi} j(\theta, t) d\theta = 2\pi D \sum_{n=1}^{+\infty} \frac{F_{0n}(r_0) k_{0n}^2 e^{-Dk_{0n}^2 t}}{C_{0n}} \quad (\text{B25})$$

as well as the total survival probability

$$S_{tot}(t) = \int_{-\pi}^{\pi} \int_a^b c(r, \theta, t) r dr d\theta = 2\pi \sum_{n=1}^{+\infty} \frac{F_{0n}(r_0) e^{-Dk_{0n}^2 t}}{C_{0n}} \quad (\text{B26})$$

from which can be inferred the typical first passage times of the process: the mean first passage time

$$\langle t \rangle = \int_0^{\infty} S_{tot}(t) dt = \frac{2\pi}{D} \sum_{n=1}^{+\infty} \frac{F_{0n}(r_0)}{k_{0n}^2 C_{0n}} \quad (\text{B27})$$

the median first passage time, t_{median} , satisfying $S_{tot}(t_{median}) = 1/2$, and the most probable first passage time, t_{prob} , for which $\frac{\partial j_{tot}}{\partial t}(t_{prob}) = 0$.

The eventual hitting probability distribution, $\tilde{J}(\theta) = \lim_{t \rightarrow +\infty} (J(\theta, t))$, can be obtained directly from the Laplace transform of $c(r, \theta, t)$:

$$\begin{aligned} \tilde{J}(\theta) &= aD \int_0^{\infty} dt \frac{\partial c}{\partial r} \Big|_{r=a} \\ &= aD \frac{\partial}{\partial r} \hat{c}(r, \theta, s) \Big|_{r=a, s \rightarrow 0} \\ &= \frac{1}{2\pi} \sum_{m=-\infty}^{+\infty} \cos(m\theta) \left(\frac{I_{m0}K'_{mb} - K_{m0}I'_{mb}}{I_{ma}K'_{mb} - K_{ma}I'_{mb}} \right) \Big|_{s \rightarrow 0} \end{aligned} \quad (\text{B28})$$

which gives Eq. (14).

In the limit of an infinitely distant confining wall, $b \rightarrow \infty$, we recover the usual unbounded expressions

$$c^*(r, \theta, t) = \sum_{m=-\infty}^{+\infty} \frac{\cos(m\theta)}{2\pi} \times \int_0^\infty \frac{e^{-Dk^2t} F_m(k, r) F_m(k, r_0)}{J_m^2(ka) + Y_m^2(ka)} k dk \quad (\text{B29})$$

with

$$F_m(k, r) = Y_m(kr) J_m(ka) - J_m(kr) Y_m(ka) \quad (\text{B30})$$

and the closure relation

$$\int_0^\infty \frac{F_m(k, r) F_m(k, r_0)}{J_m^2(ka) + Y_m^2(ka)} k dk = \frac{\delta(r - r_0)}{r_0} \quad (\text{B31})$$

for any value of m (integer).

The instantaneous flux at a specific point ($r = a, \theta$) of the absorbing inner boundary is

$$j^*(\theta, t) = \frac{D}{\pi^2} \sum_{m=-\infty}^{+\infty} \cos(m\theta) \int_0^\infty \frac{e^{-Dk^2t} F_m(k, r_0)}{J_m^2(ka) + Y_m^2(ka)} k dk \quad (\text{B32})$$

since $F'(k, a) = \frac{2}{\pi a}$. The cumulative unbounded flux then reads

$$J^*(\theta, t) = \sum_{m=-\infty}^{+\infty} \frac{\cos(m\theta)}{\pi^2} \int_0^\infty \frac{(1 - e^{-Dk^2t}) F_m(k, r_0)}{J_m^2(ka) + Y_m^2(ka)} \frac{dk}{k} \quad (\text{B33})$$

and converges to the usual expression

$$\tilde{J}^*(\theta) = \frac{1}{2\pi} \frac{1 - (a/r_0)^2}{1 - 2(a/r_0)\cos(\theta) + (a/r_0)^2} \quad (\text{B34})$$

for $t \rightarrow \infty$, the integral of which over θ giving 1 as expected.

Appendix C: Three dimensions

The concentration $c(r, \theta, t)$, $a \leq r \leq b$, $0 \leq \theta \leq \pi$, where r is the radial distance from the center of the target and θ is the polar angle (the coordinate system is chosen so that it does not depend on the azimuthal angle ϕ) obeys the following diffusion equation

$$\frac{\partial c}{\partial t'} - \frac{1}{r'^2} \frac{\partial}{\partial r'} \left(r'^2 \frac{\partial c}{\partial r'} \right) - \frac{1}{r'^2 \sin \theta} \frac{\partial}{\partial \theta} \left(\sin \theta \frac{\partial c}{\partial \theta} \right) = \frac{\delta(r' - r'_0) \delta(\theta) \delta(t')}{2\pi r'^2 \sin \theta} \quad (\text{C1})$$

which has been written in terms of the dimensionless variables $r' = r/a$ and $\tau = a^2/D$. The boundary conditions are $c(r = a, \theta, t) = 0$, $\partial c / \partial r|_{r=b} = 0$. In the remainder, we drop the primes for simplicity.

As in 2D, the solution is symmetric in θ and takes the usual form

$$c(r, \theta, t) = \sum_{m=0}^{+\infty} \left(m + \frac{1}{2} \right) P_m(\cos \theta) f_m(r, t) \quad (\text{C2})$$

with $P_m(u)$ the Legendre polynomial of degree m .

The Laplace transform of f_m obeys the differential equation

$$\frac{d^2 \hat{f}_m}{dx^2} + \frac{2}{x} \frac{d \hat{f}_m}{dx} - \left(1 + \frac{m(m+1)}{x^2} \right) \hat{f}_m = -\frac{\delta(x - x_0)}{2\pi x_0 r_0} \quad (\text{C3})$$

where the reduced variable $x = r\sqrt{s}$ has been introduced as previously.

The boundary conditions

$$\hat{f}_m(x_a) = 0 \quad \text{and} \quad \frac{\partial \hat{f}_m}{\partial x}(x_b) = 0 \quad (\text{C4})$$

imply that the global solution can be written as

$$\begin{aligned} \hat{f}_{m<}(x) &= A_m (i_m(x) k_m(x_a) - k_m(x) i_m(x_a)) \\ \hat{f}_{m>}(x) &= B_m (i_m(x) k'_m(x_b) - k_m(x) i'_m(x_b)) \end{aligned} \quad (\text{C5})$$

where $i_m(x)$ and $k_m(x)$ are the modified spherical Bessel functions of the first and second kind of order m .

Then, by continuity of \hat{f}_m and integration of Eq. (C3) across the discontinuity in x_0 , one finally gets

$$\hat{f}_m(x) = \frac{\sqrt{s} (i'_{mb} k_{m>} - k'_{mb} i_{m>}) (i_{m<} k_{ma} - k_{m<} i_{ma})}{2\pi i'_{mb} k_{ma} - k'_{mb} i_{ma}} \quad (\text{C6})$$

with $x_{<} = \min(x, x_0)$ and $x_{>} = \max(x, x_0)$, and where, for example, i'_{mb} and $k_{m>}$ stand for $\frac{\partial i_m}{\partial x}(x_b)$ and $k_m(x_{>})$.

The inverse Laplace transform and residue theorem provide the global solution in terms of dimensional variables

$$\begin{aligned} c(r, \theta, t) &= \sum_{m=0}^{+\infty} \frac{(m + \frac{1}{2}) P_m(\cos(\theta))}{2\pi i} \int_{\gamma - i\infty}^{\gamma + i\infty} ds e^{Dst} \hat{f}_m(x) \\ &= \sum_{m=0}^{+\infty} \left(m + \frac{1}{2} \right) P_m(\cos(\theta)) \sum_n \text{Res} \left[e^{Dst} \hat{f}_m(x) \right] \end{aligned} \quad (\text{C7})$$

where the sum of the residues is over the poles of \hat{f}_m , i.e. over the roots s_n of the auxiliary equation

$$g(s) = i'_m(qb) k_m(qa) - k'_m(qb) i_m(qa) = 0 \quad (\text{C8})$$

where $q = \sqrt{s}$.

The term $g'(s_n)$ appearing in the residue is

$$g'(s_n) = \frac{b}{2q_n} (i''_{mb} k_{ma} - k''_{mb} i_{ma}) + \frac{a}{2q_n} (i'_{mb} k'_{ma} - k'_{mb} i'_{ma}) \quad (\text{C9})$$

(in shorthand notation here, but evaluated in $s = s_n$), which can be simplified thanks to (C8) as

$$\begin{aligned} g'(s_n) &= \frac{b}{2q_n} \frac{i_{ma}}{i'_{mb}} (i''_{mb} k'_{mb} - k''_{mb} i'_{mb}) \\ &\quad + \frac{a}{2q_n} \frac{i'_{mb}}{i_{ma}} (i_{ma} k'_{ma} - k_{ma} i'_{ma}) \end{aligned} \quad (\text{C10})$$

Then, using the spherical Bessel identities

$$i_m(q_n a) k'_m(q_n a) - k_m(q_n a) i'_m(q_n a) = -\frac{1}{(q_n a)^2} \quad (\text{C11})$$

$$i''_m(q_n b) k'_m(q_n b) - k''_m(q_n b) i'_m(q_n b) = -\frac{(q_n b)^2 + m(m+1)}{(q_n b)^4} \quad (\text{C12})$$

the function $g'(s_n)$ reads

$$g'(s_n) = -\frac{1}{2q_n^3 a} \left(\frac{i'_{mb}}{i_{ma}} \right) - \frac{1}{2q_n^3 b} \left(\frac{i_{ma}}{i'_{mb}} \right) \left(1 + \frac{m(m+1)}{(q_n b)^2} \right) \quad (\text{C13})$$

Replacing in (C6) k'_{mb} by $i'_{mb} k_{ma}/i_{ma}$ thanks to (C8), one obtains

$$c(r, \theta, t) = \sum_{m=0}^{+\infty} \left(m + \frac{1}{2} \right) P_m(\cos(\theta)) \sum_n e^{Dq_n^2 t} \frac{a q_n^4}{\pi} \times \frac{(k_{m>} i_{ma} - i_{m>} k_{ma})(k_{m<} i_{ma} - i_{m<} k_{ma})}{1 + \frac{a}{b} \left(\frac{i_{ma}}{i'_{mb}} \right)^2 \left(1 + \frac{m(m+1)}{(q_n b)^2} \right)} \quad (\text{C14})$$

where the product $(k_{m>} i_{ma} - i_{m>} k_{ma})(k_{m<} i_{ma} - i_{m<} k_{ma})$ may also be written as $(k_{mr} i_{ma} - i_{mr} k_{ma})(k_{mr_0} i_{ma} - i_{mr_0} k_{ma})$ in terms of the initial variables r and r_0 .

Since all the solutions $q_n = \sqrt{s_n}$ of $g(s) = 0$ are purely imaginary: $q_n = i k_n$, with $k_n \in \mathbb{R}$, one can switch to the spherical Bessel functions of the first and second kind, j_m and y_m , using the relations

$$\begin{aligned} i_m(i k_n u) &= i^m j_m(k_n u) \\ i'_m(i k_n u) &= i^{m-1} j'_m(k_n u) \\ k_m(i k_n u) &= -i^{-m} [j_m(k_n u) - i y_m(k_n u)] \end{aligned} \quad (\text{C15})$$

The solution eventually takes the form

$$c(r, \theta, t) = \sum_{m=0}^{+\infty} \left(m + \frac{1}{2} \right) P_m(\cos \theta) \times \sum_{n=1}^{+\infty} e^{-Dk_{mn}^2 t} \frac{a k_{mn}^4}{\pi} \frac{f_{mn}(r) f_{mn}(r_0)}{c_{mn}} \quad (\text{C16})$$

with

$$f_{mn}(r) = y_m(k_{mn} r) j_m(k_{mn} a) - j_m(k_{mn} r) y_m(k_{mn} a) \quad (\text{C17})$$

and

$$c_{mn} = \frac{a}{b} \left(\frac{j_m(k_{mn} a)}{j'_m(k_{mn} b)} \right)^2 \left(1 - \frac{m(m+1)}{(k_{mn} b)^2} \right) - 1 \quad (\text{C18})$$

and where the k_{mn} value is the n^{th} solution of the m^{th} auxiliary equation

$$j'_m(kb) y_m(ka) - y'_m(kb) j_m(ka) = 0 \quad (\text{C19})$$

In 3D, the completeness relation of the basis functions $k_{mn}^2 f_{mn}(r) / \sqrt{c_{mn}}$ reads (whatever the value of m)

$$\frac{2a}{\pi} \sum_{n=1}^{+\infty} k_{mn}^4 \frac{f_{mn}(r) f_{mn}(r_0)}{c_{mn}} = \frac{\delta(r-r_0)}{r r_0} \quad (\text{C20})$$

while $\sum_{m=0}^{+\infty} \left(m + \frac{1}{2} \right) P_m(\cos \theta) = \delta(\theta) / \sin \theta$.

The instantaneous flux on a specific spherical strip situated at $(r = a, \theta)$ on the absorbing inner boundary is

$$\begin{aligned} j_{3D}(\theta, t) &= 2\pi a^2 D \frac{\partial c}{\partial r} \Big|_a \\ &= 2aD \sum_{m=0}^{+\infty} \left(m + \frac{1}{2} \right) P_m(\cos \theta) \\ &\quad \times \sum_{n=1}^{+\infty} \frac{k_{mn}^3 f_{mn}(r_0) e^{-Dk_{mn}^2 t}}{c_{mn}} \end{aligned} \quad (\text{C21})$$

since $\frac{\partial f_{mn}}{\partial r}(a) = 1/k_{mn} a^2$ thanks to the spherical Bessel identity (C11).

The cumulative hitting probability $J_{3D}(\theta, t) = \int_0^t j_{3D}(\theta, t') dt'$ in θ at time t is

$$\begin{aligned} J_{3D}(\theta, t) &= 2a \sum_{m=0}^{+\infty} \left(m + \frac{1}{2} \right) P_m(\cos \theta) \\ &\quad \times \sum_{n=1}^{+\infty} \frac{k_{mn} f_{mn}(r_0) (1 - e^{-Dk_{mn}^2 t})}{c_{mn}} \end{aligned} \quad (\text{C22})$$

whose integral over θ converges monotonically to 1 for $t \rightarrow \infty$ (whatever the value of r_0):

$$\int_0^\pi J_{3D}(\theta, t \rightarrow \infty) \sin \theta d\theta = 2a \sum_{n=1}^{+\infty} \frac{k_{0n} f_{0n}(r_0)}{c_{0n}} = 1 \quad (\text{C23})$$

The total flux to the inner absorbing sphere can also be computed:

$$\begin{aligned} j_{3D, \text{tot}}(t) &= \int_0^\pi j_{3D}(\theta, t) \sin \theta d\theta \\ &= 2aD \sum_{n=1}^{+\infty} \frac{f_{0n}(r_0) k_{0n}^3 e^{-Dk_{0n}^2 t}}{c_{0n}} \end{aligned} \quad (\text{C24})$$

The eventual hitting probability distribution, $\tilde{J}_{3D}(\theta)$, can be obtained directly from the Laplace transform of $c(r, \theta, t)$:

$$\begin{aligned} \tilde{J}_{3D}(\theta) &= 2\pi a^2 D \int_0^\infty dt \frac{\partial c}{\partial r} \Big|_{r=a} \\ &= 2\pi a^2 D \frac{\partial}{\partial r} \hat{c}(r, \theta, s) \Big|_{r=a, s \rightarrow 0} \\ &= \sum_{m=0}^{+\infty} \left(m + \frac{1}{2} \right) P_m(\cos \theta) \left(\frac{i_{m0} k'_{mb} - k_{m0} i'_{mb}}{i_{ma} k'_{mb} - k_{ma} i'_{mb}} \right) \Big|_{s \rightarrow 0} \end{aligned} \quad (\text{C25})$$

which gives

$$\begin{aligned} \tilde{J}_{3D}(\theta) &= \sum_{m=0}^{+\infty} \left(m + \frac{1}{2}\right) P_m(\cos \theta) \left(\frac{a}{r_0}\right)^{m+1} \\ &\times \frac{(m+1)r_0^{2m+1} + mb^{2m+1}}{(m+1)a^{2m+1} + mb^{2m+1}} \\ &> \tilde{J}_{3D}^*(\theta) \end{aligned} \quad (\text{C26})$$

in the limit of an infinitely distant wall.

The eventual hitting probability \tilde{J}_{3D} in the 3D confined system is greater than in the unbounded system, which is in stark contrast to the 2D case, and also appears in dimensions larger than 3.

- ¹K. Qiu, K.-F. Gao, L.-J. Yang, Z.-K. Zhang, R. Wang, H.-S. Ma, and Y. Jia, “A kinetic model of multiple phenotypic states for breast cancer cells,” *Scientific Reports* **7**, 9890 (2017).
- ²S. Bell and E. M. Terentjev, “Specific binding of a polymer chain to a sequence of surface receptors,” *Scientific Reports* **7**, 17272 (2017).
- ³A. Okubo and S. A. Levin, *Diffusion and Ecological Problems: Modern Perspectives* (Springer New York, 2001).
- ⁴G. M. Viswanathan, M. G. Da Luz, E. P. Raposo, and H. E. Stanley, *The physics of foraging: an introduction to random searches and biological encounters* (Cambridge University Press, 2011).
- ⁵N. Mizumoto and S. Dobata, “The optimal movement patterns for mating encounters with sexually asymmetric detection ranges,” *Scientific Reports* **8**, 3356 (2018).
- ⁶S. Mohapatra and P. S. Mahapatra, “Confined system analysis of a predator-prey minimalistic model,” *Scientific Reports* **9**, 11258 (2019).
- ⁷I. Nayak, A. Nandi, and D. Das, “Capture of a diffusive prey by multiple predators in confined space,” *Physical Review E* **102**, 062109–062116 (2020).
- ⁸A. L. Lloyd and R. M. May, “How viruses spread among computers and people,” *Science* **292**, 1316–1317 (2001).
- ⁹C. C. Wang, K. A. Prather, J. Sznitman, J. L. Jimenez, S. S. Lakdawala, Z. Tufekci, and L. C. Marr, “Airborne transmission of respiratory viruses,” *Science* **373**, 981–992 (2021).
- ¹⁰L. Lu, R. S. Sikkema, F. C. Velkers, D. F. Nieuwenhuijs, E. A. J. Fischer, P. A. Meijer, N. Bouwmeester-Vincken, A. Rietveld, M. C. A. Wegdam-Blans, P. Tolsma, M. Koppelman, L. A. M. Smit, R. W. H. van der Honing, W. H. M. van der Poel, A. N. van der Spek, M. A. H. Spierenburg, R. J. Molenaar, J. de Rond, M. Augustijn, M. Woolhouse, J. A. Stegeman, S. Lycett, B. B. O. Munnink, and M. P. G. Koopmans, “Adaptation, spread and transmission of sars-cov-2 in farmed minks and associated humans in the netherlands,” *Nature Communications* **12**, 6802–6813 (2021).
- ¹¹Y. Zhang and O. K. Dudko, “First-passage processes in the genome,” *Annual Review of Biophysics* **45**, 117–134 (2016).
- ¹²P. Kar, A. G. Cherstvy, and R. Metzler, “Acceleration of bursty multiprotein target search kinetics on DNA by colocalisation,” *Physical Chemistry Chemical Physics* **20**, 7931–7946 (2018).
- ¹³P. E. Schavemaker, A. J. Boersma, and B. Poolman, “How important is protein diffusion in prokaryotes?” *Frontiers in Molecular Biosciences* **5**, 93–108 (2018).
- ¹⁴A. Erbaş and J. F. Marko, “How do dna-bound proteins leave their binding sites? the role of facilitated dissociation,” *Current Opinion in Chemical Biology* **53**, 118–124 (2019).
- ¹⁵M. Stracy, J. Schweize, D. J. Sheratt, A. N. Kapanidis, S. Uphoff, and C. Lesterlin, “Transient non-specific dna binding dominates the target search of bacterial dna-binding proteins,” *Molecular Cell* **81**, 1499–1514 (2021).
- ¹⁶S. Redner, *A Guide to First-Passage Processes* (Cambridge University Press, 2001).
- ¹⁷A. J. Bray, S. N. Majumdar, and G. Schehr, “Persistence and first-passage properties in nonequilibrium systems,” *Advances in Physics* **62**, 225–361 (2013).
- ¹⁸P. C. Bressloff and J. M. Newby, “Stochastic models of intracellular transport,” *Reviews of Modern Physics* **85**, 135–196 (2013).
- ¹⁹R. Metzler, G. Oshanin, and S. Redner, *First-Passage Phenomena and Their Applications* (World Scientific, 2014).
- ²⁰O. Bénichou and R. Voituriez, “From first-passage times of random walks in confinement to geometry-controlled kinetics,” *Phys. Rep.* **539**, 225–284 (2014).
- ²¹A. Godec and R. Metzler, “First passage time distribution in heterogeneity controlled kinetics: going beyond the mean first passage time,” *Scientific Reports* **6**, 20349 (2016).
- ²²J. Koplik, S. Redner, and E. Hinch, “Tracer dispersion in planar multipole flows,” *Physical Review E* **50**, 4650 (1994).
- ²³J. Koplik, S. Redner, and E. Hinch, “Universal and nonuniversal first-passage properties of planar multipole flows,” *Physical review letters* **74**, 82 (1995).
- ²⁴S. Condamine, O. Bénichou, V. Tejedor, R. Voituriez, and J. Klafter, “First-passage times in complex scale-invariant media,” *Nature* **450**, 77–80 (2007).
- ²⁵O. Bénichou, C. Chevalier, J. Klafter, B. Meyer, and R. Voituriez, “Geometry-controlled kinetics,” *Nature Chemistry* **2**, 472–477 (2010).
- ²⁶G. Vaccario, C. Antoine, and J. Talbot, “First-passage times in d -dimensional heterogeneous media,” *Phys. Rev. Lett.* **115**, 240601 (2015).
- ²⁷O. Bénichou, T. Guérin, and R. Voituriez, “Mean first-passage times in confined media: from markovian to non-markovian processes,” *Journal of Physics A Mathematical and Theoretical* **48**, 1630001–1630043 (2015).
- ²⁸A. Godec and R. Metzler, “Universal proximity effect in target search kinetics in the few-encounter limit,” *Physical Review X* **6**, 041037 (2016).
- ²⁹D. S. Grebenkov, “Universal formula for the mean first passage time in planar domains,” *Physical Review Letters* **117**, 260201–260204 (2016).
- ³⁰D. S. Grebenkov, “Subdiffusion in a bounded domain with a partially absorbing-reflecting boundary,” *Physical Review E* **81**, 021128 (2010).
- ³¹T. Guérin, M. Dolgushev, O. Bénichou, and R. Voituriez, “Universal kinetics of imperfect reactions in confinement,” *Communications chemistry* **4**, 157–163 (2021).
- ³²Z. Schuss, A. Singer, and D. Holcman, “The narrow escape problem for diffusion in cellular microdomains,” *Proceedings of the National Academy of Sciences* **104**, 16098–16103 (2007).
- ³³D. Holcman and Z. Schuss, “The narrow escape problem,” *SIAM Review* **56**, 213–257 (2014).
- ³⁴D. S. Grebenkov, R. Metzler, and G. Oshanin, “Full distribution of first exit times in the narrow escape problem,” *New Journal of Physics* **21**, 122001–122022 (2019).
- ³⁵C. W. Hong and Q. Zeng, “Tapping the treasure of intracellular oncotargets with immunotherapy,” *FEBS Letters* **588**, 350–355 (2013).
- ³⁶N. J. Yang and M. J. Hinner, “Getting across the cell membrane: An overview for small molecules, peptides, and proteins,” in *Site-Specific Protein Labeling* (Springer New York, 2014) p. 29–53.
- ³⁷“Boundary issues,” *Cell: Boundary Issues* **165**, 759–761 (2016).
- ³⁸E. I. Ozay, G. Gonzalez-Perez, J. A. Torres, J. Vijayaraghavan, R. Lawlor, H. L. Sherman, D. T. Garrigan, A. S. Burnside, B. A. Osborne, G. N. Tew, and L. M. Minter, “Intracellular delivery of anti-pPKC θ (thr538) via protein transduction domain mimics for immunomodulation,” *Molecular Therapy* **24**, 2118–2130 (2016).
- ³⁹S. Miersch and S. S. Sidhu, “Intracellular targeting with engineered proteins,” *F1000Research* **5**, 1947 (2016).
- ⁴⁰I. Trensveska, D. Li, and A. H. Banham, “Therapeutic antibodies against intracellular tumor antigens,” *Frontiers in Immunology* **8**, 1001 (2017).
- ⁴¹Y. Lanoiselée, N. Moutal, and D. S. Grebenkov, “Diffusion-limited reactions in dynamic heterogeneous media,” *Nature Communications* **9**, 4398 (2018).
- ⁴²P. Sil, N. Mateos, S. Nath, S. Buschow, C. Manzo, K. G. N. Suzuki, T. Fujiwara, A. Kusumi, M. F. Garcia-Parajo, and S. Mayor, “Dynamic actin-mediated nano-scale clustering of cd44 regulates its meso-scale organization at the plasma membrane,” *Molecular Biology of the Cell* **31**, 561–579 (2020).
- ⁴³R. W. Taylor, C. Holler, R. G. Mahmoodabadi, M. Küppers, H. M. Dastjerdi, V. Ziburdaev, A. Schambony, and V. Sandoghdar, “High-precision protein-tracking with interferometric scattering microscopy,” *Frontiers in Cell and Developmental Biology* **8**, 590158–590178 (2020).
- ⁴⁴H. Carslaw and J. Jaeger, *Conduction of heat in solids* (Oxford: Clarendon

- Press, 1959).
- ⁴⁵J. Crank, *The mathematics of diffusion* (Oxford university press, 1975).
- ⁴⁶J. P. Holman, *Heat Transfer* (McGraw-Hill, 1990).
- ⁴⁷T. Bickel, "A note on confined diffusion," *Physica A: Statistical Mechanics and its Applications* **377**, 24–32 (2007).
- ⁴⁸C. Antoine and J. Talbot, "Nonintuitive interplay between confinement and dimensionality for angle-resolved first passage statistics," *Physical Review Research* **2**, 012019 (2020).
- ⁴⁹D. S. Grebenkov, "Spectral theory of imperfect diffusion-controlled reactions on heterogeneous catalytic surfaces," *The Journal of Chemical Physics* **151**, 104108 (2019).
- ⁵⁰D. S. Grebenkov, "Diffusion toward non-overlapping partially reactive spherical traps: Fresh insights onto classic problems," *The Journal of Chemical Physics* **152**, 244108 (2020).
- ⁵¹D. S. Grebenkov, "Surface hopping propagator: An alternative approach to diffusion-influenced reactions," *Physical Review E* **102**, 032125 (2020).
- ⁵²D. S. Grebenkov, "Paradigm shift in diffusion-mediated surface phenomena," *Physical Review Letters* **125**, 078102 (2020).
- ⁵³G. Pólya, "Über eine aufgabe der wahrscheinlichkeitsrechnung betreffend die irrfahrt im straßennetz," *Mathematische Annalen* **84**, 149–160 (1921).